Volume 16, Issue 3, 162517 (1-14)

International Journal of Nano Dimension (IJND)

https://dx.doi.org/10.57647/j.ijnd.2025.1603.17

Green-synthesized titanium dioxide nanoparticles with pyrogallol functionalization: A novel approach using cow dung extract for anticancer applications

Sancharan Acharya[1], Akanksha Behera[1], Aswathy CS[1], Sujatha Venugopal[2], Ramesh Thiyagarajan[3], Thirunavukkarasu Chinnasamy[1,*]

[1]*Department of Biochemistry and Molecular Biology, Pondicherry University, Kalapet, Puducherry, Puducherry, India.*
[2]*DST-Mobility Fellow, Department of Chemistry, Pondicherry University, Kalapet, Puducherry, Puducherry, India.*
[3]*Department of Basic Medical Sciences, College of Medicine, Prince Sattam Bin Abdulaziz University, Al-Kharj, Kingdom of Saudi Arabia.*

[*]**Corresponding author:** tarasu.bbm@pondiuni.edu.in

Original Research

Received:
2 September 2024
Revised:
17 December 2024
Accepted:
20 January 2025
Published online:
1 June 2025

Abstract:

Growing interest has been shown in the environment friendly synthesis of metal nanoparticles, yet no published research exists on synthesizing titanium dioxide nanoparticles (TiO_2NPs) using cow dung extract (CD). In this manuscript, we synthesized TiO_2NPs using CD extract (CD-TiO_2) and functionalized them with pyrogallol (P-CD-TiO_2). The physicochemical characteristics of the TiO_2NPs were evaluated using UV-Vis spectroscopy, dynamic light scattering, Fourier-transform infrared spectroscopy, Raman spectroscopy, X-ray photoelectron spectroscopy, X-ray diffraction and scanning electron microscopy. The qualitative analysis of CD extract and biological activities of CD-TiO_2 and P-CD-TiO_2 were evaluated. The potential anticancer activity was examined *in vitro* against Hep3B using the MTT assay. The hydrodynamic size of CD-TiO_2 and P-CD-TiO_2NPs were 147.9 nm and 183.4 nm, respectively. The CD-TiO_2 and P-CD-TiO_2 were spherical in shape, with an average size ranging from 32 nm to 48 nm. CD-TiO_2 and P-CD-TiO_2 showed anti-hemolytic, anti-inflammatory, antioxidant activity, and significant cytotoxicity against Hep3B cells. The IC_{50} of CD-TiO_2 was 379.9 μg/mL, while P-CD-TiO_2 showed a significantly higher cytotoxicity with an IC_{50} of 31.98 μg/mL. The results revealed that CD extract is an effective reducung agent for TiO_2 nanoparticles synthesis. Notably, the green-synthesized P-CD-TiO_2 NPs exhibited promising anticancer potential in concentration-dependent manner while being safe for red blood cells.

Keywords: Cow dung; Green synthesis; Hepatocellular carcinoma; Nanoparticles; Pyrogallol; Titanium dioxide

1. Introduction

Cancer is a malignant, intricate, and globally prevalent disease. Among its many forms, hepatocellular carcinoma (HCC) ranks fifth globally in terms of cancer occurrence rate. After lung cancer, HCC is the second most prevalent cause of cancer-related mortality among men [1]. Liver-directed therapy, surgery, chemotherapy, and liver transplantation are the methods used to treat HCC patients; nevertheless, there are very few options for treating the incurable HCC. The systemic therapy of advanced HCC has been approved for tyrosine kinase inhibitors such as lenvatinib and sorafenib; however, after extended use, these drugs acquire chemoresistance, making systemic chemotherapy less prevalent. Furthermore, individuals with advanced HCC may also have additional liver-related abnormalities, which reduce their acceptability for systemic chemotherapy [2]. Thus, it is imperative to create novel medications that can treat cancer without causing toxicity or adverse consequences. As a result, a great deal of current research in cancer treatment applications has focused on nanomaterials, which are recognized for their size-related characteristics and biocompatibility in tumor detection and prevention [3, 4]. Recently, nanoparticles have gained attention in the

green nanobiotechnology field due to their potential biomedical applications. Such metal oxide nanoparticles derived from transition metals like TiO_2, CuO, ZnO, ZnS, CdS, etc., exhibit unique physical, chemical, electrical and optical properties and possess a high ratio of surface area to volume [5]. Among these, titanium dioxide (TiO_2) is a cheap, non-hazardous and inert substance. It has high refractive index as well as high capacity to absorb UV light spectra. These exceptional qualities have caused TiO_2 to become more and more popular since the early 20th century. It occurs in three different forms: rutile, brookite, and anatase [6]. They are used in a wide variety of applications, including solar cells, photocatalysis, self-cleaning surfaces, and antibacterial agents in water treatment [7]. Photocatalytic wastewater treatment employs nano-sized TiO_2 as a highly effective means of breaking down and getting rid of refractory organic and inorganic impurities [8]. The physical and chemical procedures of production involve significant time and financial investment, as well as the use of dangerous chemicals, high temperatures and pressures to accomplish the target, which restricts their ability to be manufactured, and also restricts its uses in possible medical applications due to higher toxicity [9]. As a result, one method that is often utilized to produce less toxic and biologically active nanoparticles is green synthesis. For large-scale nanoparticle synthesis, green synthesis methods offer a naturally flexible, ecologically responsible, and economically viable alternative. Furthermore, the biocompatibility of green synthesized TiO_2 nanoparticles is appreciable as hepatocytes recognize the surface of TiO_2, which is similar to a hierarchically extended collagen nanofibrillar surface. These nanoparticles govern and regulate the expression of several hepatic proteins, including cytochrome P450, albumin, and transferrin [10]. TiO_2 nanoparticles have the ability to slow the growth of breast cancer MDA-MB 231 cells, according to earlier research by Latha et al. 2017 [11]. It has been demonstrated by Zhang et al. 2004 that the photocatalytic activity of TiO_2-mediated toxicity eliminates cancer cells [12]. Endocytosis has been found to be the mechanism by which TiO_2 nanoparticles interact with cell membranes and enter cells [13].

It's interesting to note that cow dung, which is naturally comma after abundant has also been investigated as a possible source for green synthesis, demonstrating the variety of ways in which ecologically beneficial techniques like this might be used in the synthesis of nanoparticles [14]. Cow dung is the undigested remnants of food that is excreted from the alimentary canal after being processed by the gut microbiota of the cow. As studies have shown that it is a rich source of nutrients, minerals, fibers, and other phytoconstituents, it can be repurposed wisely without wasting. Many constituents present in cow dung make it a cheap, biodegradable, readily available rich source of microflora. As the cow grazes on plants and grasses, its fecal matter is abundant in phytoconstituents like phenolic compounds, alkaloids, flavonoids, etc. such phytochemicals can simultaneously serve as reducing, stabilizing, or capping agents during the green synthesis of nanoparticles [15]. The plants synthesize them as secondary metabolites and are involved in pathogen defense [16]. Cow dung-based nanoparticle synthesis is a novel area of research. Javed et al. 2023 uniquely used cow dung extract to synthesize zinc oxide nanoparticles, marking the only known instance using this approach demonstrating promising agricultural applications [14].

Studies reported that surface functionalization of nanoparticles changes the physical and biological properties of nanoparticles [17, 18]. Pyrogallol is a catechin compound, a polyphenol isolated from certain plant species namely tea (Camella sinensis). It is known to have anti-cancer properties [19]. Pyrogallol is chemically a benzenetriol, soluble in water, highly reactive to oxygen (giving it a brownish appearance). It is a known generator of superoxide anion, and also known to play a role in apoptosis and cell cycle arrest via reactive oxygen species (ROS) production [20]. The green synthesis of silver nanoparticles mediated by pyrogallol and its impact on biofilm and cytotoxicity studies were carried out before by Sampath et al. 2021, where the pyrogallol conjugated silver nanoparticles showed the potential anti-microbial and anti-cancer activities [21]. There are only a few studies that have used pyrogallol for surface functionalization of nanoparticles. No studies are yet reported with pyrogallol conjugated TiO_2 nanoparticles, especially via cow dung-based synthesis method. Thus, the present study focuses on TiO_2 nanoparticles synthesized using cow dung extract (CD-TiO_2) and functionalizing pyrogallol on the surface of these nanoparticles to enhance their biological properties for medicinal applications. In light of the pervasive threat posed by cancer, our study sought to harness the potential of cow dung-derived nanoparticles, especially the pyrogallol functionalized ones (P-CD-TiO_2) in combating this complex and widespread disease.

2. Materials and methods

2.1 Materials

All chemicals were of molecular biology grade and were purchased from HiMedia, India. MTT, DMEM, amphotericin and chloramphenicol solution were purchased from Sigma Aldrich Pvt Ltd, India.

2.2 Cow dung extract preparation

Fresh cow dung, collected from a dairy farm near Pondicherry University, Chinna Kalapet (12° 0.97′N 79° 51.33′E), was continuously dried under sunlight for three days. The obtained dried cakes of cow dung were finely powdered using a mortar and pastle. It was stored at 25 °C in a tightly sealed plastic container for further use. Weighing out 10 g of the powdered dry cow dung, we combined it with 100 mL of Milli-Q water. After that, it was boiled in a conical flask without cover at 100 ºC for 15 minutes on a hotplate and left to cool at room temperature. Whatman No. 1 filter paper was used for filtering after it was centrifuged for 15 minutes at 11000 rpm. After that, the collected supernatant was kept in an airtight container, which, when kept at 25 ºC, could be utilized for up to three days.

2.3 Synthesis of CD-TiO_2 and P-CD-TiO_2 nanoparticles

The cow dung mediated synthesis of TiO_2 nanoparticles was standardized by varying time, temperature, concentration of cow dung extract and TiO_2, and pH of the reaction mixture. The yield and hydrodynamic shell size (Z_{Avg}) of the synthesized nanoparticles were set as the parameters for standardization. 25 mM TiO_2 solution was prepared in Milli-Q water and stirred at 40 ºC using a magnetic stirrer. 10% aqueous cow dung extract was slowly added to the reaction container with continuous stirring. 1:5 ratio of cow dung extract to TiO_2 solution was finally achieved, where a color change from pure white to brownish white was seen. Stirring was continued for two hours at 40 ºC. After 2 hours, the reaction mixture was left at room temperature to cool, transferred in centrifuge tube, and centrifuged at 12000 rpm for 15 minutes. The supernatant was disposed, the brownish-white pellet was washed using Milli-Q water, and centrifugation was done at 11000 rpm for 10 minutes. The washing process was repeated twice, and pellets were collected in a petri plate. It was placed inside a hot air oven at 90 ºC overnight. Dried nanoparticles were scraped and finely ground with a mortar and a pestle. The yield was measured and it was stored in an airtight container for later use. The similar standardization approach was followed for P-CD-TiO_2 nanoparticles. After adding the cow dung extract in 1:5 ratio, equal volume of 25 mM aqueous pyrogallol solution was added and stirred continuously for 2 hours in the dark. Dark condition is required, due to the light sensitive nature of pyrogallol solution. After 2 hours, the nanoparticles from the solution were obtained in pure, by following the same purification protocol mentioned above for CD-TiO_2.

2.4 Phytoconstituents screening of cow dung extract

Mayer's test and Hager's test were done to test alkaloids as described by Kancherla, et al. 2019 [22]. Ferric chloride test was performed to test flavonoids [23]. Gelatin test, Ferric chloride test and Iodine test were done to test for phenolic compounds [24, 25] .

2.5 Characterization of nanoparticles

CD-TiO_2 and P-CD-TiO_2 nanoparticles were characterized to determine the particle size, crystalline nature, surface functional groups, elemental composition, and surface morphology using various spectrometric techniques described as follows.

2.5.1 UV-vis spectrometry

Stored CD-TiO_2 and P-CD-TiO_2 nanoparticles were weighed and dissolved in Milli-Q water for making the end concentration of 100 μg/mL. The samples were then probe sonicated for 2 minutes to make it a homogeneous suspension. 100 μL of this suspension was diluted with 900 μL of Milli-Q water to reduce the optical density errors caused by high absorbance of TiO_2. The prepared samples were analyzed using Shimadzu 3600 spectrophotometer, to obtain the optical spectra within a range of $200-700$ nm. Band gap energy of CD-TiO_2 and P-CD-TiO_2 were calculated from the obtained UV data using Tauc equation.

2.5.2 Particle size analyzer–dynamic light scattering (DLS)

The hydrodynamic sizes of CD-TiO_2 and P-CD-TiO_2 nanoparticles were estimated using the Malvern Zeta Sizer Nano S. In water, stored CD-TiO_2 and P-CD-TiO_2 nanoparticles were dissolved to achieve 1 mg/mL concentration, probe sonicated for 2 minutes, and spun for 30 seconds. The upper layer was collected to avoid the interference of agglomerated particles. The solution was again sonicated using a path sonicator for at least 15 minutes before performing the analysis.

2.5.3 Raman spectroscopy

The powdered sample was used for the Raman spectroscopic analysis, which needs to be filled in the small piths of metallic microscopic slides. The Raman spectroscopic analysis was done within a range of $0-1600$ cm^{-1} wavenumber using Laser Confocal Raman Microscope with Spectrometer, Renishaw Metrological Systems UK (Model: Invia Reflex Raman microscope with spectrometer).

2.5.4 X-ray photoelectron spectroscopy (XPS)

XPS analysis was done with Thermo Scientific K-Alpha-KAN9954133 for examining the elements present in the surface with a binding energy in the range of $0-1300$ eV. The drop casting method was used to produce the sample for XPS examination. The thick slurry of the CD-TiO_2 and P-CD-TiO_2 nanoparticles were prepared using isopropanol and were cast onto a small piece of glass slide. The glass slides were allowed to dry before analysis.

2.5.5 X-ray diffraction (XRD)

XRD data was obtained using Rigaku Ultima IV X-ray diffractometer within 2θ values ranging from $10-80°$. The powdered specimen was used for XRD analysis. The measurement parameter settings include 30 mA, 40 kV, and 25°. The anode material used is copper (Cu) and the K-Alpha1 value is 1.54060° A. The particle size was obtained using the Scherrer formula.

2.5.6 Fourier-transform infrared spectroscopy (FTIR)

FTIR analysis was done with Thermo Nicolet 6700 spectrophotometer within the range of $400-4000$ cm^{-1}. The FTIR sample used for analysis was thin transparent potassium bromide (KBr) pellets mixed with the CD-TiO_2 and P-CD-TiO_2 nanoparticles. The moisture content from the sample and KBr were removed by keeping under infrared light source. The background correction was done with KBr pellets (the reference sample). The FTIR spectra of cow dung and pyrogallol alone were also obtained to ensure the functional group incorporation into the nanoparticles.

2.5.7 Scanning electron microscopy (SEM)

SEM analysis was done using Hitachi of Model number S-340 Scanning electron microscope. The nanoparticles were dried into powder, finely ground and mounted onto a sample holder. The images were analyzed using Image J software.

2.6 Biological activity

For all the biological activity assays, first the nanoparticles were sterilized by autoclaving them in powder form and then the suspensions were prepared using appropriate solvents.

2.6.1 Hemolytic activity

Cytotoxic effect was studied by performing a hemolysis test as stated by Liaqat et al. 2022 with slight modifications [26]. In brief, 1 mL of Avian red blood cells (RBCs) suspension and 100 μL of nanoparticle solution in PBS of varying concentrations (800, 400, 200, 100, 50, 25, 12.5, 6.25, 3.12, 1.56 μg/mL) was put into a microcentrifuge tube. The tubes underwent incubation for 35 minutes at 37 ºC with intermittent agitations every 10 minutes. After cooling for 5 minutes at room temperature, it was centrifuged for 5 minutes at 1000 rpm. After collecting the supernatant, the absorbance at 576 nm was measured. The positive control was 0.1% v/v of triton-X100, while the negative control was PBS buffer at 7.4 pH.

2.6.2 Anti-inflammatory activity

Lopez-Miranda et al. 2023 procedure for *in vitro* anti-inflammatory activity was followed with a few modifications [27]. Briefly, 500 μL of various concentrations (1.56, 3.12, 6.25, 12.5, 25, 50, 100, 200, 400, 800 μg/mL) of CD-TiO_2 and P-CD-TiO_2 nanoparticles in distilled water taken in microcentrifuge tubes were mixed with 450 μL of 1% BSA solution. It was incubated at 37 ºC for 30 minutes and heated at 70 °C for 20 minutes. These were then allowed to cool, and the absorbance was obtained by a microplate reader at 660 nm. Distilled water and diclofenac sodium (DFS) of the same sample concentration and volume served as control and standards respectively.

2.6.3 DPPH assay

DPPH free radical scavenging activity of CD-TiO_2 and P-CD-TiO_2 was measured by the method followed by Sampath et al. 2020, including small modifications [21]. Briefly, 2.7 mL of 0.1 mM DPPH in methanol and 0.3 mL of varying concentrations (0.625, 1.25, 2.5, 5, 10, 20, 40 μg/mL) of test solutions prepared using distilled water–cow dung, standard (vitamin C), CD-TiO_2, and P-CD-TiO_2 were mixed well in reaction tubes. The tubes were incubated in dark for an hour, and absorbance measured at 517 nm. The methanol without test solutions served as the positive control.

2.6.4 Nitric oxide scavenging activity

The protocol was processed with slight modification as previously described Rajakumar et al. 2018 [28]. Briefly, 1 mL sodium nitroprusside solution and 1 mL of sample solution were added to the reaction tubes and then incubated at 25 ºC for 150 minutes. Following that, 2 mL of Griess reagent was added, and an absorbance reading at 546 nm was made. The various concentrations (1.5625, 3.125, 6.25, 12.5, 25, 50, 100, 200, 400, 800 μg/mL) of CD-TiO_2 and P-CD-TiO_2 prepared in distilled water, were compared with the same concentrations of cow dung extract and standard vitamin C for their radical scavenging efficiency. As a positive control, PBS buffer is used in which no test samples are added to the reagents.

2.6.5 Ferric reducing power assay (FRAP)

Fe^{3+} reduction antioxidant ability was done for CD-TiO_2 and P-CD-TiO_2 according to Solaiman et al. 2020 with slight modifications [29]. 1 mL of nanoparticle suspension of varying concentrations (1.56, 3.12, 6.25, 12.5, 25, 50, 100, 200, 400, 800 μg/mL) in distilled water, 1 mL phosphate buffer solution, and 1 mL potassium ferricyanide were pipetted into centrifuge tubes and incubated at 50 ºC for 20 minutes. After quickly chilling these, 1% ice-cold trichloroacetic acid (TCA) solution was added to the reaction mixture. After centrifuging the tubes for ten minutes at 3000 rpm, 1 mL of the supernatant was combined with the same amount of Milli-Q water. After adding 1 mL of 1% ferric chloride solution, the absorbance at 700 nm was measured with a microplate reader. In place of the nanoparticle dispersion, 1 mL of phosphate buffer served as the negative control and vitamin C as the positive control.

2.6.6 MTT assay-cell viability test on Hep3B cell line

The cytotoxicity of the nanoparticles was evaluated as a percentage of cell viability using colorimetric 3-(4,5-dimethyl-2-thiazolyl)-2,5-diphenyl-2H-tetrazolium bromide (MTT) assay as mentioned in Ezhuthupurakkal et al. (2018) [30]. The cytotoxic IC_{50} values were calculated using graphical method by curve fitting analysis. Briefly, Hep3B cells were seeded in 96-well cell culture plate in a way that each well contained approximately 5×10^4 cells. The plates were incubated for 24 hours at 37 ºC, 5% CO_2 to reach 80% confluency. The culture medium was removed, and the cells were washed with PBS in all wells. Varying concentrations of CD-TiO_2 and P-CD-TiO_2 nanoparticle suspensions in PBS (12.5, 25, 50, 100, 200, 400 μg/mL) were added to the wells, only PBS without any nanoparticles was added to the control well. The plate was re-incubated in dark condition. 24 hours post-treatment, cytotoxicity was determined using tetrazolium dye. 10 μL (0.5 mg/mL) of MTT was added to all wells, incubated for 3 hours at 37 ºC, 5% CO_2. After 3 hours, the wells were thoroughly washed with PBS (3 times), the formazan crystals formed were dissolved in 100 μL DMSO. The cell viability was recorded using microplate reader at 570 nm.

2.6.7 Morphological studies on Hep3B cell line

Hep3B cells were observed after nanoparticle treatment in the cell viability assay. Hep3B cells treated with Doxorubicin in this instance were used as a positive control. Cells were analyzed under a microscope (Olympus CX40, USA) at 40x magnification.

2.7 Statistical analysis

All the experiments/assays were performed in triplicates and repeated thrice, the results are shown in mean $\pm$ SD, and the statistical analysis were done using GraphPad Prism software version 9.5.1. ANOVA followed by Tukey test was followed for all the biological assays, except for hemolytic and cell viability assay which used student's t-test to determine the statistical significance of our sample.

3. Results and discussion

3.1 Phytochemical study

Table 1 displays all of the qualitative phytochemical analysis results. According to Gelatin test, Ferric chloride test, Iodine test, the aqueous portion of the crude extract in this investigation yielded positive results for the presence of flavonoids, phenolic compounds (supplementary Fig. S1). The aqueous extract of cow dung was discovered to contain flavonoids and polyphenols. The total phenolic content in 10% cow dung extract was estimated to be 233.7 ± 11.098 GAE/g of extract. The total flavonoid content in 10% cow dung extract was determined to be 99.35 ± 3.05 CAT/g of extract. The standard curve and the data obtained are depicted in supplementary graph S1 & S2 and Table S1 and S2.

3.2 Characterization of nanoparticles

3.2.1 UV-visible spectroscopy

UV-visible spectral analysis from $200 - 700$ nm showed a single peak at 240 nm for CD-TiO_2, The P-CD-TiO_2 nanoparticles showed two absorption maxima at different wavelengths. An additional broad peak at 400 nm is visible for P-CD-TiO_2 apart from the peak observed at 240 nm, shown in Fig. 1 (A). The Tauc plots for both nanoparticles are also shown in Figs. 1 (B) & (C).

3.2.2 Dynamic light scattering (DLS)

With a PDI of 0.084, the hydrodynamic size of the CD-TiO_2 nanoparticles was found to be 147.9 nm. Figs. 1 (D) and (E), depicts size distribution of CD-TiO_2 and P-CD-TiO_2 nanoparticles respectively, suspended in Milli-Q water. P-CD-TiO_2 showed slightly increased hydrodynamic shell size (Fig. 1 (E)) of 183.4 nm with a PDI of 0.251.

3.2.3 Raman spectroscopy

Five vibrational modes were obtained, after Raman spectroscopy. All five-characteristic shift in the Raman spectra matches with the assigned vibrational modes of anatase TiO_2. Five prominent peaks are obtained at wavenumbers 144 cm^{-1}, 519 cm^{-1}, 399 cm^{-1}, 197 cm^{-1}, and 639 cm^{-1} for CD-TiO_2 nanoparticles which represents active modes of anatase phase TiO_2. Similar five vibrational modes were obtained for P-CD-TiO_2 with only slight variations. The peaks obtained for P-CD-TiO_2 are at wavenumbers 147 cm^{-1}, 516 cm^{-1}, 398 cm^{-1}, 197 cm^{-1} and 638 cm^{-1} and are also associated with the three Eg modes, two B1g modes and one A1g mode of anatase TiO_2 nanoparticles. The Raman spectra of CD-TiO_2 and P-CD-TiO_2 with the vibrational modes assigned for each peak is shown in Figs. 2 (A) & (B), respectively.

3.2.4 X-ray photoelectron spectroscopy (XPS)

Figs. 2 (C) & (D), depicts, d lower case the data obtained from XPS analysis. Four prominent elements, namely Carbon, nitrogen, titanium, and oxygen were obtained from the surface layer of CD-TiO_2 and P-CD-TiO_2 nanoparticles. In case of CD-TiO_2, the peaks obtained are for Ti 2p, C 1s, N 1s, and O 1s with atomic ratios of 9.41%, 58.33%, 1.45%, and 30.8% respectively. Similar peak positions are obtained for P-CD-TiO_2 at Ti 2p, C 1s, N 1s, and O 1s with their respective atomic ratios 47.4%, 2.33%, 10.83%, and 39.42%. The partial XPS spectra of Ti 2P showed peaks at 458.6 eV, 464.4 eV, and 472.2 eV for CD-TiO_2. Overlapping peaks at same binding energy exists for P-CD-TiO_2 also. O 1s XPS spectrum showed two prominent peaks at binding energies 532.4 eV and 529.8 eV for CD-TiO_2. The binding energies of P-CD-TiO_2 for O 1s partial spectra, is slightly shifted to higher intensity as compared to CD-TiO_2. C 1s spectra showed two peaks at 284.9 eV and 289 eV for both CD-TiO_2 and P-CD-TiO_2 nanoparticle at two different intensities (supplementary Fig. S2).

3.2.5 X-ray diffraction (XRD)

Figs. 2 (E) & (F), depicts sharp diffraction patterns of same intensities for both CD-TiO_2 and P-CD-TiO_2 nanoparticles. The dominant peaks obtained are at 2θ positions $-24.8°$, 37.3°, 47.6°, 53.4°, 54.7°, and 62.4°for CD-TiO_2 and 24.4°, 37.01°, 47.2°, 53.2°, 54.37°, and 62.1° for P-CD-TiO_2. For CD-TiO_2, the average crystalline size was determined to be 40.3 nm, while for P-CD-TiO_2, it was 39.2 nm. More detailed descriptions of the XRD data of the nanoparticles are given in supplementary Table S3 & S4.

3.2.6 Fourier transform infrared spectroscopy (FTIR)

FTIR results obtained from cow dung, pyrogallol, CD-TiO_2 and P-CD-TiO_2 are depicted below in the Fig. 3 (A). The prominent FTIR peaks of cow dung that are incorporated into the CD-TiO_2 and P-CD-TiO_2 are seen at 3460 cm^{-1}, 2928 cm^{-1}, 1639 cm^{-1}, 1230 cm^{-1}, etc. FTIR peaks of pyrogallol that are also seen with the FTIR spectra of CD-TiO_2 and P-CD-TiO_2 at 3454 cm^{-1}, 1891 cm^{-1}, 1737 cm^{-1}, and

Table 1. Qualitative phytochemical analysis of aqueous cow dung extract.

Phytoconstituents	Phytochemical test	Observation	Result
Alkaloids	Mayer's test	No white precipitate was observed	Negative
	Hager's tests	No yellow precipitate	Negative
Flavonoids	Ferric chloride test	The brown color was developed	Positive
Phenolic compounds	Gelatin test	No white precipitate was found	Negative
	Ferric chloride test	Greenish–brown color was developed	Positive
	Iodine test	The transient red color was formed	Positive

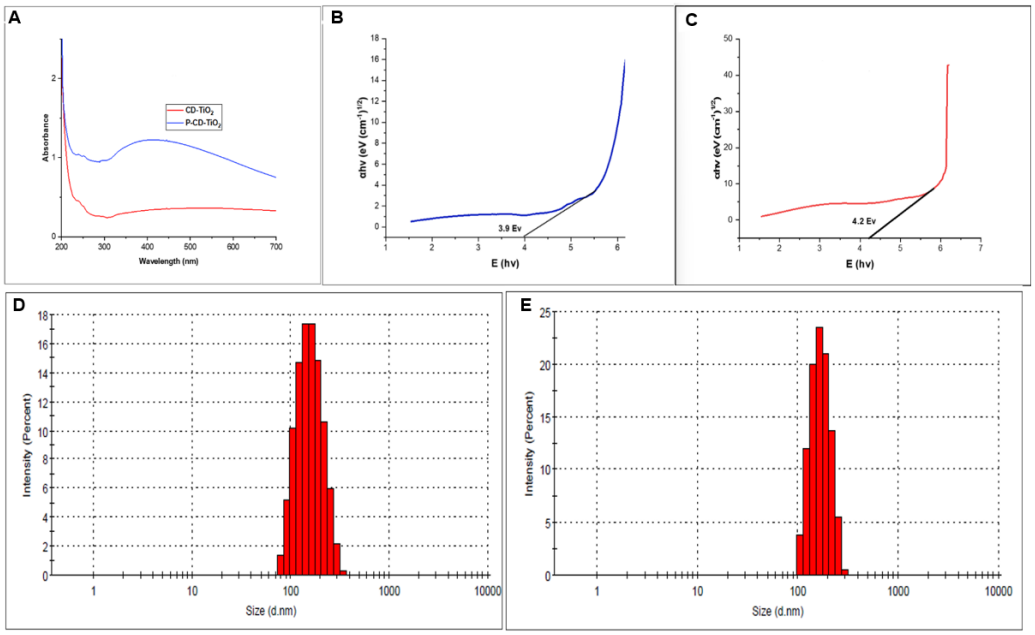

Figure 1. (A) UV-vis spectra of CD-TiO_2 (red line) and P-CD-TiO_2 (blue line) nanoparticles. (B) Tauc plot for CD-TiO_2 nanoparticles (C) Tauc plot for P-CD-TiO_2 nanoparticles. (D) Size distribution of CD-TiO_2. (E) Size distribution of P-CD-TiO_2.

1524 cm^{-1}. The characteristic dominating peaks exclusively have been seen with CD-TiO_2 and P-CD-TiO_2 at 821 cm^{-1} and 815 cm^{-1}, respectively.

3.2.7 Scanning electron microscopy (SEM)

The scanning electron microscopic analysis of samples showed that both CD-TiO_2 and P-CD-TiO_2 exhibited more or less spherical shapes in its nanoforms. The average sizes were calculated and are found to be 39.9 nm for CD-TiO_2 and 40.3 nm for P-CD-TiO_2. The images are shown in Figs. 3 (B) and (C).

3.3 Biological activities

3.3.1 Hemolytic activity

The green synthesized nanoparticles showed less hemolytic activity with chicken erythrocytes. The CD-TiO_2 and P-CD-TiO_2 nanoparticles exhibit no significant difference in their hemolytic potential when compared. CD-TiO_2 nanoparticles showed the highest hemolytic potential of $2.7 \pm 0.039\%$ at 800 μg/mL concentration, compared to the P-CD-TiO_2 nanoparticles with a hemolytic potential of $2.68 \pm 0.08\%$ at the same concentration. The % hemolytic activity decreased in a dose-dependent manner, as demonstrated in Fig. 4 (A).

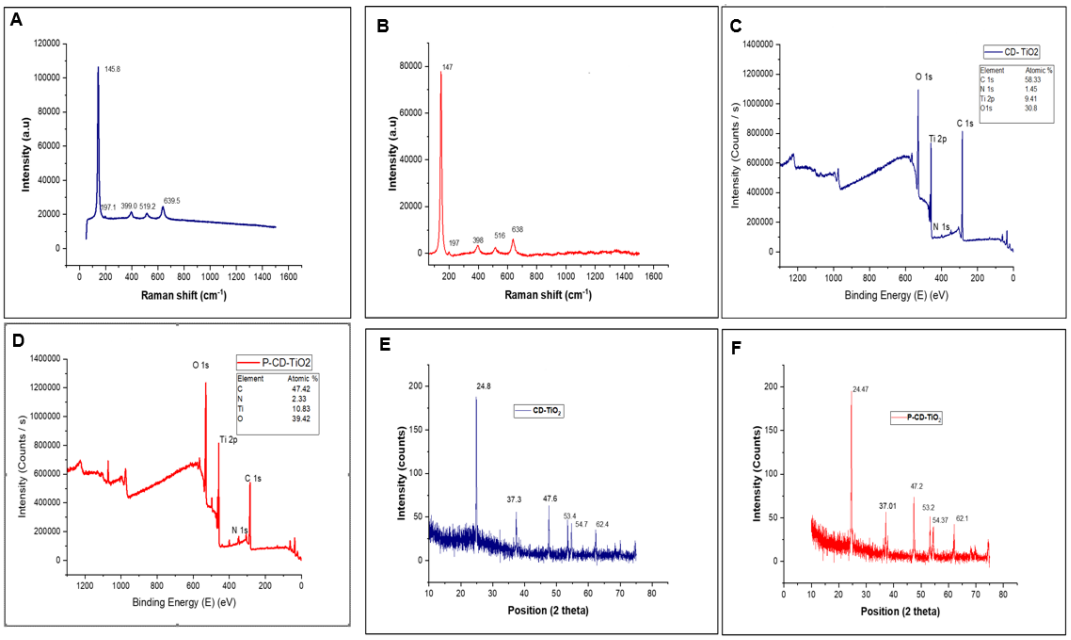

Figure 2. (A) Raman spectra of CD-TiO_2. (B) Raman spectra of P-CD-TiO_2, (C) XPS full spectra of CD-TiO_2 (D) XPS full spectra of P-CD-TiO_2 nanoparticles; (E) XRD data depicting the anatase phase of CD-TiO_2 nanoparticles and (F) XRD data depicting the anatase phase of XRD data depicting the anatase phase of P-CD-TiO_2 nanoparticles.

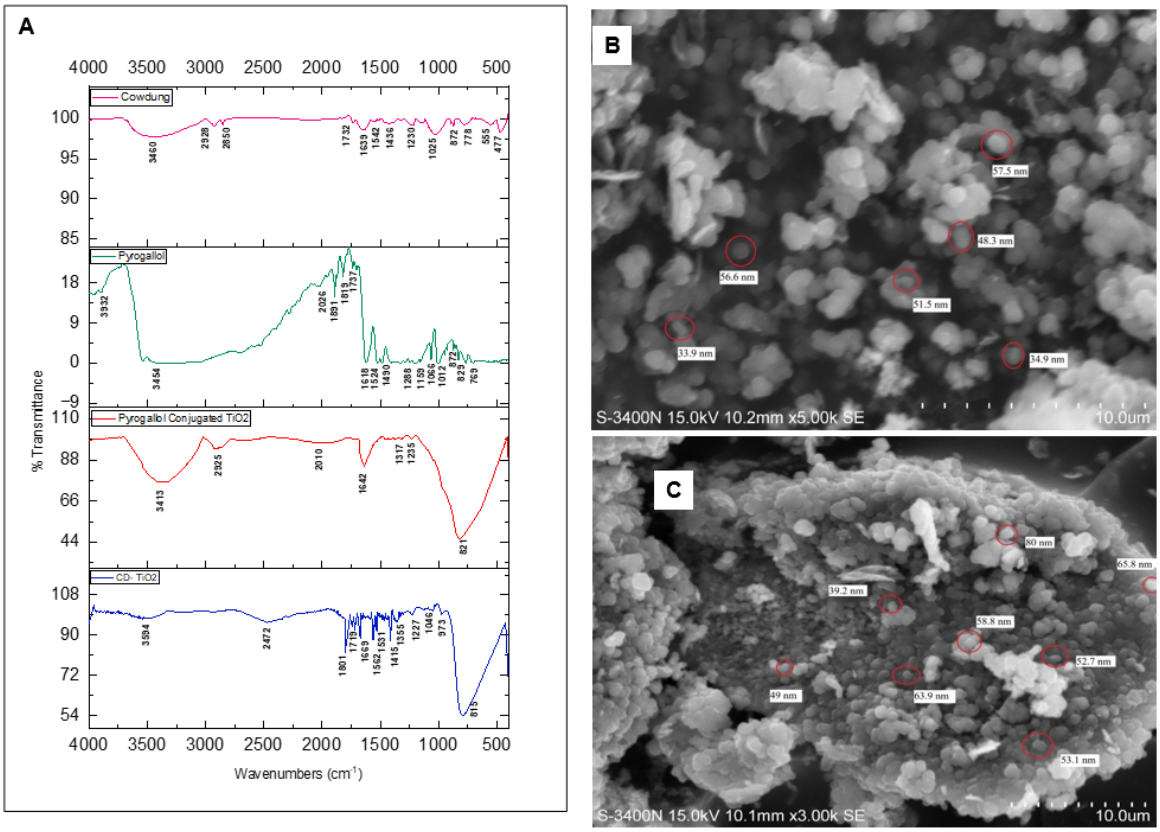

Figure 3. (A) FTIR spectra obtained for cow dung, pyrogallol, P-CD-TiO_2 and CD-TiO_2 respectively; (B) SEM images of synthesized CD-TiO_2; and (C) SEM images of synthesized P-CD-TiO_2 nanoparticles.

More detailed descriptions are given in supplementary Table S5.

3.3.2 Anti-inflammatory activity

TiO_2 nanoparticles have a protective effect on protein denaturation. The highest nanoparticle concentration (800 μg/mL) shows 41% inhibition, and the lowest concentration of 1.56 μg/mL confers 99% protection to proteins. Comparing these results with P-CD-TiO_2 nanoparticles, the protective effect on protein denaturation is enhanced at a higher concentration (800 μg/mL) to 70%. The lowest concentration showed similar activity of 99% inhibition of denaturation. Moreover, our nanoparticles showed identical protective effects compared to reference drug DFS. Fig. 4 (B) shows the findings of the comparison analysis.

3.3.3 DPPH radical scavenging assay

The DPPH free radicals produced in the process can be scavenged by CD-TiO_2 and P-CD-TiO_2 nanoparticles. The highest scavenging activity was observed for 10 μg/mL concentration of both CD-TiO_2 and P-CD-TiO_2, 78%, and 87%, respectively. IC_{50} of the CD-TiO_2 and Pyrogallol conjugated CD-TiO_2 are calculated to be 6 μg/mL and 2.19 μg/mL respectively. As compared to the standard, there is no significant activity, observed for cow dung. A statistically significant higher scavenging activity is observed for CD-TiO_2. P-CD-TiO_2 showed comparable activity with that of the vitamin C standard with no significant difference between them. The more detailed comparative analysis is depicted using Fig. 4 (C).

3.3.4 Nitric oxide scavenging assay

Fig.. 4 (D) shows the highest percentage activity of 84% and 74% were obtained for CD-TiO_2 and P-CD-TiO_2 at 10 μg/mL concentration. CD-TiO_2 and P-CD-TiO_2 showed statistically comparable nitric oxide scavenging activity. Compared to the vitamin C activity, CD-TiO_2 nanoparticle suspension exhibited significantly higher scavenging property. Our cow dung extract showed significantly less nitric scavenging compared to vitamin C.

3.3.5 Ferric reducing power assay (FRAP)

Fig. 5 (A), depicts FRAP analysis on both CD-TiO_2 and P-CD-TiO_2 which shows significantly higher ferric reducing power when compared to the cow dung extract. Significant ferric reducing activities were found between CD-TiO_2 and P-CD-TiO_2 nanoparticles at 100 μg/mL and 50 μg/mL concentrations. More detailed descriptions are given in supplementary Table S6.

3.3.6 Cell viability test on Hep3B cell lines

MTT assay on Hep3B cell lines, showed reasonable cytotoxic effects of CD-TiO_2, and more profound cytotoxic ability for P-CD-TiO_2 (Fig. 5 (B)). The IC_{50} of CD-TiO_2 showed at 379.9 μg/mL. Surprisingly P-CD-TiO_2 showed significantly high cytotoxic nature than that of CD-TiO_2 with an IC_{50} at 31.98 μg/mL ($p < 0.05$). More detailed descriptions are given in supplementary Table S7.

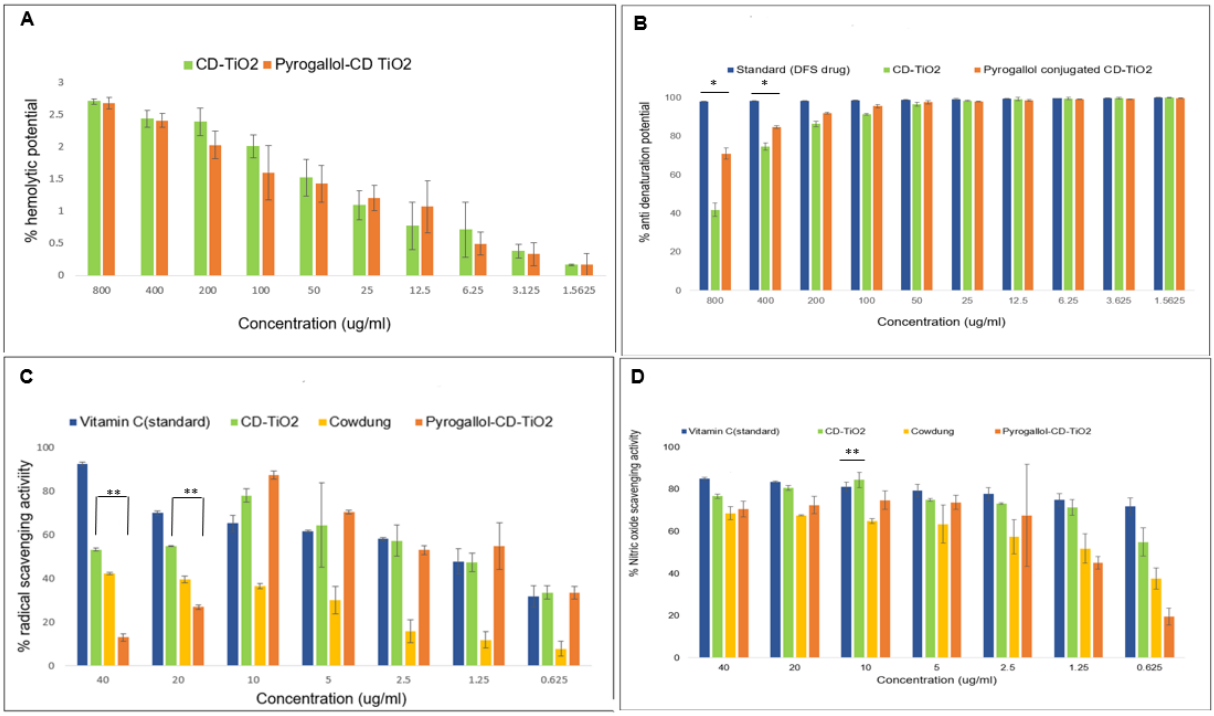

Figure 4. (A) Hemolytic activity of green synthesized CD-TiO_2 & P-CD-TiO_2 nanoparticles using chicken RBC. No significant difference was found between the CD-TiO_2 and P-CD-TiO_2 nanoparticles ($p < 0.05$) (B). Comparative analysis of anti-denaturation potential of green synthesized CD-TiO_2 and P-CD-TiO_2. At higher doses, our nanoparticles showed significant difference between the protective effects when compared to reference drug DFS (*$p < 0.05$) (C). Comparative analyses of radical scavenging activity of CD-TiO_2 and P-CD-TiO_2 nanoparticles with cow dung extract and standard vitamin C. As compared to the standard, there is no significant activity for cow dung. Statistically significant higher scavenging activity is observed for CD-TiO_2 (**$p < 0.01$) compared to P-CD-TiO_2. (D). Nitric oxide radical scavenging activity of CD-TiO_2 and P-CD-TiO_2. Both the nanoparticles showed statistically comparable nitric oxide scavenging activity. Compared to the vitamin C activity, CD-TiO_2 nanoparticle suspension exhibited significantly higher scavenging property (**$p < 0.01$) at the concentration 10 μg/mL. The results are shown in mean $\pm$ SD.

3.3.7 Impact of P-CD-TiO_2- and CD-TiO_2 nanoparticles on the morphology of cells

The cells in control group and groups treated with lower concentrations such as 12.5 and 25 μg/mL, didn't show any significant change in morphology. At higher concentrations, such as 200 and 400 μg/mL, most of the cells had a shrunken morphology and were spherical in shape (Fig. 6 and Fig. 7).

Prior to the green synthesis and characterization of TiO_2 nanoparticles, a preliminary phytochemical analysis was done to determine the biological source that can act as the reducing, capping, and stabilizing agents present in the aqueous cow dung extract. The qualitative analysis showed the presence of phenolic compounds and flavonoids. Further, the total phenolic and total flavonoid content estimation confirmed that phenolic content in the 10% cow dung extract was higher compared to the flavonoids present. Javed et al. (2022) synthesized zinc oxide nanoparticles using cow

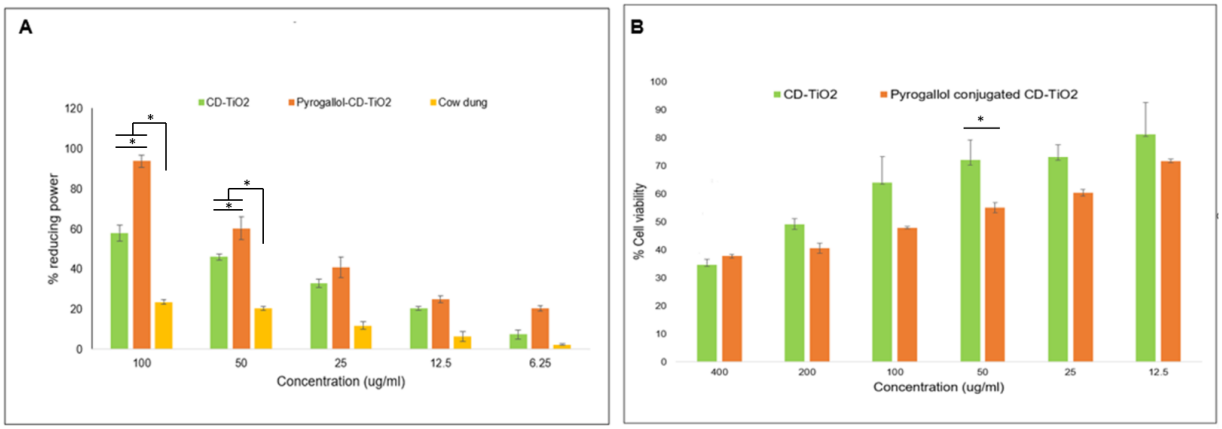

Figure 5. (A) Ferric reducing antioxidant power of CD-TiO_2, P-CD-TiO_2 nanoparticles and cow dung extract. The results are shown in mean $\pm$ SD (*$p < 0.05$). (B) The cytotoxic effect of CD-TiO_2 and P-CD-TiO_2 on Hep3B cell line. The results are shown in mean $\pm$ SD. The percentage cell viability was assessed by MTT assay. The IC_{50} of CD-TiO_2 showed at 379.9 μg/mL. P-CD-TiO2 showed the IC_{50} at 31.98 μg/mL which is significantly higher compared to CD-TiO2 (*$p < 0.05$).

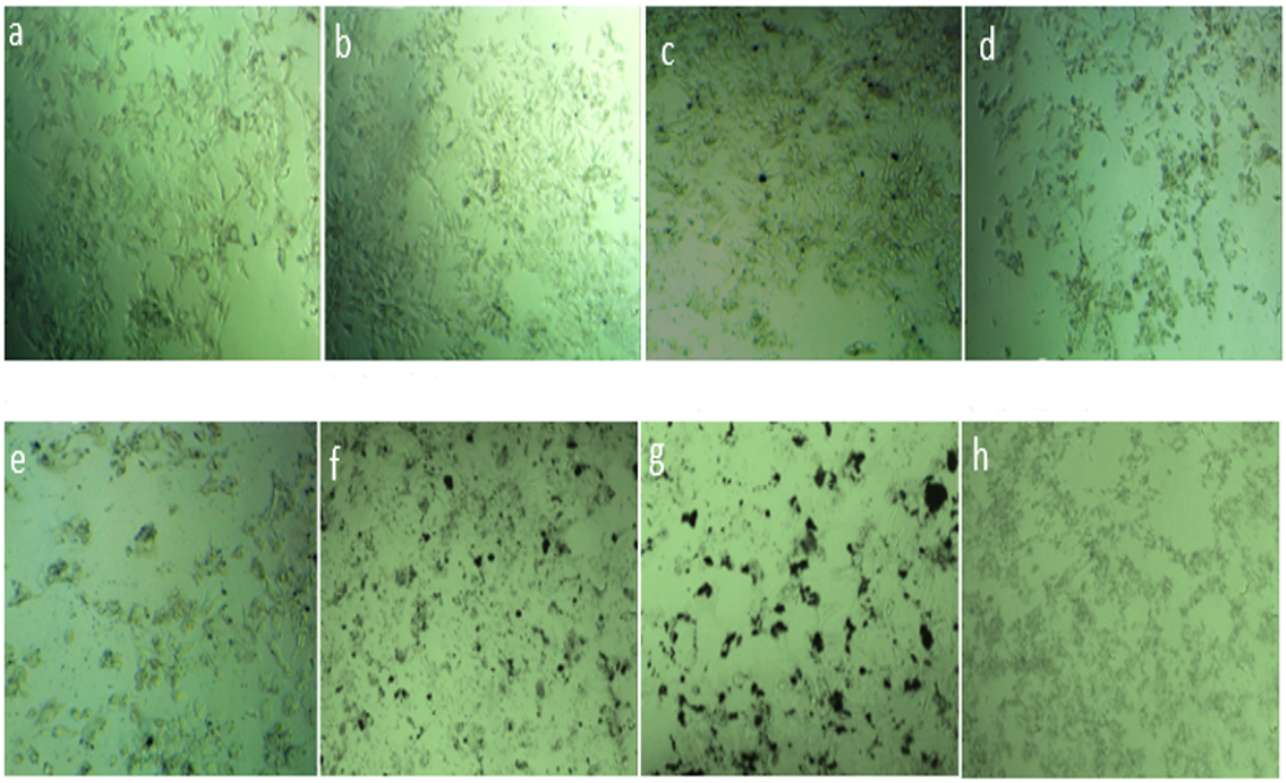

Figure 6. The light microscopic view of viable cell under each CD-TiO_2 treated wells compared with control. (a) control, (b) 12.5 μg/mL, (c) 25 μg/mL, (d) 50 μg/mL, (e) 100 μg/mL, (f) 200 μg/mL, (g) 400 μg/mL, (h) doxorubicin.

dung extract, and found 0.12 μg/mL of phenolic content in it which is less than the amount estimated in our sample [14]. This may be due to differences in the food source, metabolic activity, and gut microbes of the cow from which the cow dung was obtained.

UV-visible spectrum of CD-TiO_2 and P-CD-TiO_2 showed prominent absorption at regions below 450 nm. Previous UV data of TiO_2 nanoparticles synthesized by green route reported wide range of absorption maxima in the UV region. *Trigonella foenum* leaf extract-mediated TiO_2 synthesis produced peaks at 400 nm [31], while *Echinacea purpurea* herbal extract has an absorption spectra at 280 nm [32]. An absorption spectra between $200-300$ nm were observed for Aloe vera extract mediated TiO_2 nanoparticles [33]. All those data clearly indicated the wide spectrum of absorption for TiO_2. The wavelength at which the synthesized nanoparticles shows maximum peak depends on the size of the nanoparticle, rate of agglomeration, nanoparticle stability, etc. [33]. The calculated band gap energy of both CD-TiO_2 and P-CD-TiO_2 is greater that the bulk TiO_2 (Eg = 3.20 eV) [5]. The increase in band gap energy reflects the decrease in size of the nanoparticle being synthesized. In bulk material, large number of atoms and molecule cluster together, overlapping their orbitals with each other, this decreases the energy gap between conduction band and valence band and attributes to its electrical conductivity. As the particle size decreases towards nanoscale, number of overlapping orbitals decrease, the width of the bands gets narrower causing increase in band gap energy between conduction band and valence band. The band gap is the forbidden area for electron, the larger bandgap; more electrons are restricted in the forbidden region. This accounts for its lower conductivity, and lower ROS production of the nanoparticle than from bulk material. Previous research has shown that TiO_2 can neutralize ROS and reactive nitrogen species (RNS) that are released by inflammatory cells when they act as mediators of the inflammatory response [34].

The hydrodynamic diameter of CD-TiO_2 and P-CD-TiO_2 were observed to be 147 nm and 183 nm respectively with PDI values of 0.08 and 0.25 respectively. Generally the size determined by DLS is large when compared to the size obtained from SEM due to the hydrodynamic shell around the nanoparticles [5]. Astonishingly commercially purchased TiO_2 are found to have larger hydrodynamic diameter ranging from $400-1000$ nm, and may be due to the poor capping or stabilizing agent present in the reaction media unlike green synthesis methods [35]. The less PDI value, or narrow size distribution may also be controlled by biogenic reducing agent present during the synthesis [36].

Anatase TiO_2's six vibrational modes were reproduced using Raman spectroscopy. Tetragonal structure characterizes anatase. Two primitive cells, each containing two TiO_2 atoms, make up each conventional cell. Our CD-TiO_2 and P-CD-TiO_2 nanoparticles exhibit the Raman active modes of anatase TiO_2 at 2B1g (399 cm^{-1} and 519 cm^{-1}), A1g (519 cm^{-1}), and 3Eg (144 cm^{-1}, 197 cm^{-1}, 639 cm^{-1}). The phonon confinement model indicated slight shift in these peaks towards right side due to the decreased size of nanoparticles. The bulk TiO_2 has same six vibrational modes at 196 cm^{-1}, 143 cm^{-1}, 514 cm^{-1}, 396 cm^{-1}, and 637 cm^{-1} from which CD-TiO_2 and P-CD-TiO_2 showed a light right shiftiness. The nanoscale reduction of size from

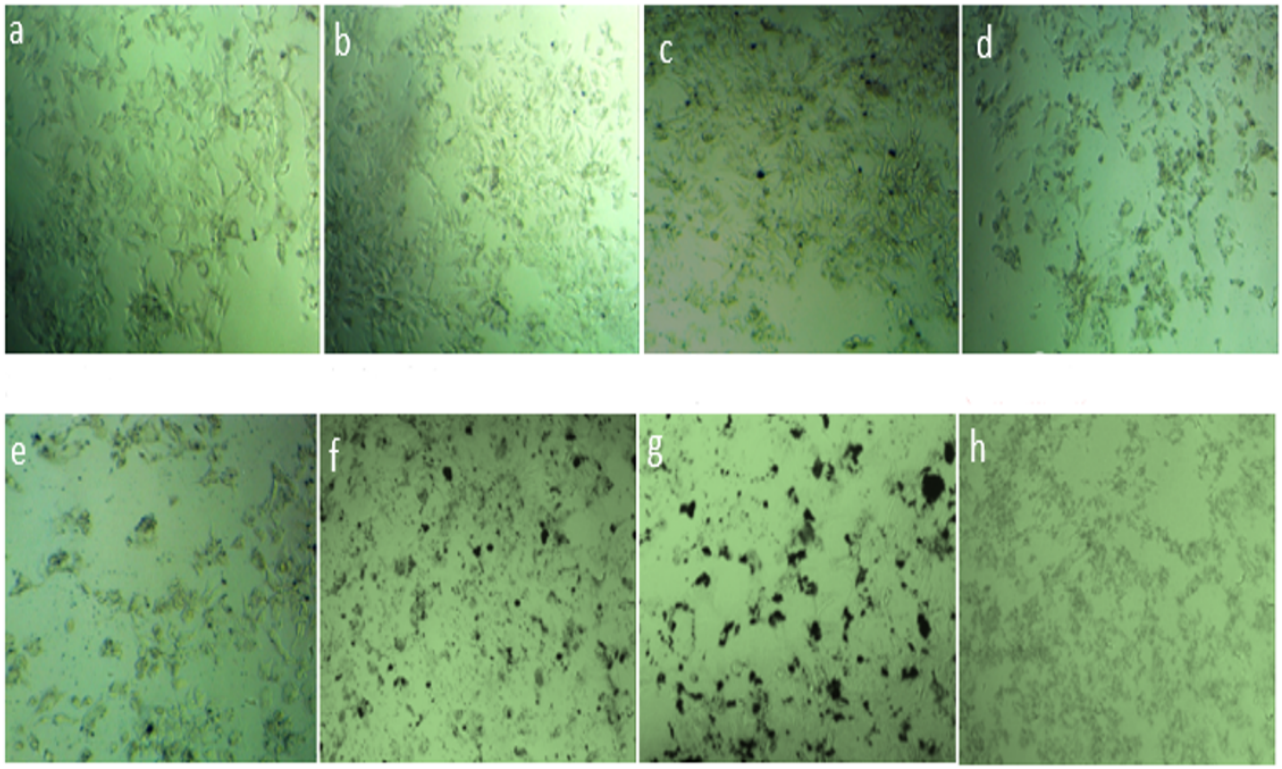

Figure 7. The light microscopic view of viable cell under each P-CD-TiO_2 treated wells compared with control. (a) control, (b) 12.5 μg/mL, (c) 25 μg/mL, (d) 50 μg/mL, (e) 100 μg/mL, (f) 200 μg/mL, (g) 400 μg/mL, (h) doxorubicin.

bulk salt affects the vibrational properties to some extent. Mainly, volume contraction occurs due to size induced radial pressure, decreasing the interatomic distances. The volume contraction is the main reason for the shift in vibrational modes from bulk material and the nanoparticles [37]. XPS analysis, inferred that the surface layer of synthesized nanoparticles contains titanium, carbon, oxygen, and nitrogen. According to the peak fitting areas and from previous studies we may infer that, there exist Ti-O bonds (458 eV and 472 eV) at the surface for CD-TiO_2 and P-CD-TiO_2 nanoparticles that belonged to TiO_2. The two dominant peaks in O 1s matched for O-Ti (529.9 eV), and C-O or O-H (531.5 eV). From peak fitting analysis of previous literatures concluded that the two dominating peaks in C 1s partial spectra belong to aromatic carbon (284 eV) and C-Ti-O bonds (289 eV). The absence of C 1s peaks at binding energies 454.9 eV (Ti-C bonds) and 282 eV, 281.6 eV (C-Ti bonds), indicates that titanium's chemical environment does not change and that carbon does not enter the anatase phase. The slightly increased intensities for P-CD-TiO_2 say that the C-O, and O-H bonds are more on the nanoparticle surface than that of the CD-TiO_2. It may serve as an indirect evidence for pyrogallol functionalization at the surface [38]. All the obtained peaks obtained from XRD for both CD-TiO_2 and P-CD-TiO_2 are assigned for anatase phase of TiO_2. The peaks represent the corresponding miller indices 24.8° (101), 37.2° (004), 47.2° (200), 53.2° (015), 54.2° (105), 62.1° (204) and showed good agreement with the JCPDS card No. 21-1272 [32]. The XRD data showed that the sample is 100% in its anatase phase with tetragonal lattice structure with an average crystalline size of 40 nm. Previous studies say that green approach for nanoparticles resulted in thermodynamically stable anatase phase when compared to chemical processes adopted [39].

FTIR spectra of the cow dung extract and pyrogallol revealed that it contains necessary functional groups required for the conversion of bulk TiO_2 to TiO_2 nanoparticles, its stabilization and capping. The hydroxyl functional groups found in phenolic compounds exhibit significant stretching vibrations, which correlate to the intense band at $3300 - 3550$ cm^{-1}. 2928 cm^{-1} and 2850 cm^{-1} peaks for cow dung extract represents the C=O and -OH- stretching vibrations aromatic and carbonyl groups of proteins present in the cow dung extract (positive test for amino acids and proteins). The peaks at 1737 cm^{-1} and 1618 cm^{-1} for pyrogallol and 1639 cm^{-1} and 1732 cm^{-1} for cow dung are attributed to C=O of amide bonds [40]. These functional groups can easily drive the bio-reduction process of TiO_2 to form nanoscale titanium dioxide particles. The saturated hydrocarbons showed FTIR peaks at 1542 cm^{-1} and 1524 cm^{-1} for cow dung and pyrogallol respectively [41]. The abovementioned peaks are nearly replicated in the CD-TiO_2 and P-CD-TiO_2 FTIR peaks also, that tells us those moieties are actually acting as the reducing, stabilizing and capping agents for TiO_2 nanoparticle synthesis. The most important peaks, exclusively found in CD-TiO_2 and P-CD-TiO_2 are at 821 cm^{-1} and 815 cm^{-1} which are the unique bands assigned for Ti-O stretching, Ti-O-Ti vibrational stretches [42]. The FTIR observations are in accordance with the observations of XPS, in terms of the elemental composition and chemical bonds present.

SEM analysis showed that the CD-TiO_2 and P-CD-TiO_2

are spherical shaped with the size ranging from $32-48$ nm. The calculated SEM image size is in agreement with the crystalline size obtained from XRD data.

The drugs and pharmaceutical compounds are tested for their *in vitro* hemolytic potential during the preliminary phase of the pre-clinical trial. Our CD-TiO_2 and P-CD-TiO_2 nanoparticles have less hemolytic activity. Hence these are considered biocompatible and safe to use. Our results align with the caffeic acid-based TiO_2 nanoparticles synthesized by Chahardoli et al. 2022 where 1.5% hemolysis was observed for their highest concentration of 500 μg/mL [43]. According to previous literature, chemically synthesized TiO_2 nanoparticles of Mahalakshmi and Vijaya et al. 2021 showed 51% hemolysis, which is far from our results [44]. It indicated the less toxic effect of our nanoparticles and proved the efficiency of green synthesized nanomaterials to prevent unwanted hemolysis. Similarly, our nanoparticles have $87-98$% anti-hemolytic effects, that are appreciable and are similar to the green synthesized TiO_2 nanoparticle functionalized with marigold [45]. The phenolic and flavonoid functional groups that are bonded to the surface of green synthesized nanoparticles obtained from biogenic sources may be the cause of the protective actions of these particles on erythrocytes [46].

The substantial surface area to volume ratio of nanoparticles is attributed to their properties of blocking inflammation enhancers like cytokines and pro-inflammatory enzymes. The titanium dioxide nanoparticles synthesized via the green route are found to exhibit anti-inflammatory properties [47]. The *in vitro* screening of the anti-inflammatory action of CD-TiO_2 and P-CD-TiO_2 nanoparticles using the BSA denaturation technique analyzes nanoparticles' ability to prevent protein denaturation. The assay is vital to screen for a drug and reduce its side effects and other medical complications. Our CD-TiO_2 and P-CD-TiO_2 nanoparticles are highly efficient, showing the highest protective result at their lowest concentration. This may be due to the synergistic action of antioxidant activity of the nanoparticles at lower concentrations. Higher doses hinder nanoparticles' protective denaturation effect. P-CD-TiO_2 showed a significantly higher protective effect for BSA denaturation due to the functionalized catechol groups at the surface of the nanoparticles [21].

Oxidative stress occurs when the body undergoes physiological stress as a part of metabolic reactions and as well as due to exposure to various chemicals and toxic agents. A balance between ROS scavengers and ROS producers needs to be established to prevent the harmful effects of oxidative stress. An imbalance results in the disruption of the reduced environment inside the cellular system. Excessive production of free radicals is capable of damaging DNA, proteins, lipids, resulting in diseases like cancer, diabetes, etc. Compared to the previous studies of the radical scavenging potential of TiO_2 using various plant extracts, cow dung-based synthesis confers significant antioxidant potential as low as 10 μg/mL concentrations [48]. The polyphenol functionalization may have augmented the antioxidant activity of CD-TiO_2 nanoparticles. Pyrogallol conjugation can give additional capping effects with their catechol groups and may be the reason behind enhanced DPPH radical scavenging activity compared to CD-TiO_2 [21]. Surprisingly, we also found that the antioxidant action starts to decrease at higher concentrations above 10 μg/mL. One possible explanation is that the number of electrons released from the TiO_2 exceeds the concentration required to neutralize the free radicals. These excess electrons may be antagonizing the radical scavenging properties at higher concentrations [49]. Considering the reducing power antioxidant activity of CD-TiO_2 and pyrogallol conjugated CD-TiO_2 nanoparticles, pyrogallol functionalization has augmented the activity significantly. The catechol group capping may be the underlying reason that renders the nanoparticles suspension to reduce more ferric to ferrous iron form [21]. The *in vitro* antioxidant assays confirmed that cow dung mediated TiO_2 nanoparticle synthesis exhibited a good electron-donating capacity to stabilize the free radicals formed and can also scavenge the nitric oxide radicals in the reaction system. They also have the potential to maintain the Fe^{3+}-Fe^{2+} equilibrium so that radical generation can be controlled to some extent. The balance between ferrous and ferric forms of iron is essential in the biological system.

The IC_{50} values of CD-TiO_2 and Pyrogallol conjugated nanoparticles respectively showed comparable effects with the previous literatures of MTT assay performed on various other cell lines like Gastric adenocarcinoma cell lines, HepG2, etc. [21, 33]. Another study of Green synthesized TiO_2 nanoparticles on colorectal carcinoma cell lines showed IC_{50} values at $300-400$ μg/mL. From the previous cytotoxic analysis of biogenic TiO_2 nanoparticles, it is evident that the cytotoxic potential varies, and are influenced by factors like, type of cell lines used, number of cells seeded in each well, source of extract used for synthesis, and nanoparticle concentration. As far as we're aware of, cytotoxic potential of CD-TiO_2 nanoparticles were not studied on Hep3B cell lines so far. Our Conjugated CD-TiO_2 with pyrogallol has augmented its effect and decreased its IC_{50} values significantly indicating the anti-cancer enhancing potential after pyrogallol capping. Oncology researchers are tirelessly working to establish novel anti-cancer drugs, or to enhance the anti-cancer efficacy of new drugs. As the nanoparticles are close in size of biological mediators, they can easily penetrate through the cells, and attributes for its drug delivering efficiency. Surface functionalization can facilitates its immune system evasion, or can enhance its target binding [50]. This may be the reason for the enhanced anti-cancer effect of pyrogallol conjugated CD-TiO_2 nanoparticles. Anti-hemolytic assay assured that the above-mentioned cytotoxic concentrations are not causing significant hemolysis to the erythrocytes.

We then looked at how cell morphology was affected by CD-TiO_2 and P-CD-TiO_2 nanoparticles. The morphologic characteristics of the cells may be the indicator of cell death. The quantity of round-shaped cells was greater at 400 μg/mL than in cells subjected to 12.5, 25, 50, 100, or 200 μg/mL. The observations coincide with the data of cell viability assay and previous studies also, as Wang et al. (2015) observed wrinkles appeared on and around the spherical cell when 200 μg/mL TiO_2 nanoparticles were present.

A concentration-dependent way revealed typical apoptotic morphological alterations of cell shrinkage in response to TiO_2 nanoparticles treatment in A549 cells, suggesting that TiO_2 nanoparticles trigger apoptosis in A549 cells [51]. According to another study, at greater concentrations of TiO_2 nanoparticles (100 μg/mL), A375 cell line showed cell shrinkage, nuclear condensation, fragmentation, and cell debris were also seen [52].

As per the result of cell viability assay and morphological analysis we tried to speculate the reason for cell deaths. In a study it has been found that by activating the caspase-8/Bid pathway, TiO_2 nanoparticles cause JB6 cell apoptosis; the process of apoptosis may involve damage to the permeability of the mitochondrial membrane [53]. Hence it can be speculated that the cell deaths could be because of apoptosis by activating the caspase-8/Bid pathway or damage to the permeability of the mitochondrial membrane. In another study G1 phase of the cell cycle was arrested in colon cancer cells by TiO_2 nanoparticles [54]. So, the reason for cell deaths in our study could be cell cycle arrest also. As these nanoparticles are showing anti-inflammatory effect which may be because of ROS scavenging, it suggests that cell death by mitochondrial damage due to ROS generation might not be the possible reason [55]. The food, health, and environmental conditions of the animals can all affect the chemical makeup of cow dung extract. This lack of standardization may have an impact on the synthesis process's reproducibility; to overcome this problem a more thorough chemical analysis of the cow dung extract is needed. Since the anticancer efficacy was solely evaluated *in vitro*, the findings may not be immediately applicable to clinical settings or *in vivo* systems. Because the study does not sufficiently assess the nanoparticles' long-term biocompatibility or toxicity to healthy cells, safety concerns may arise. Further studies on normal cell lines and cancer cell lines for screening apoptotic markers, cell cycle analysis, and DNA damage are required to understand the full mechanism of cytotoxic killing by our nanoparticles along with *in vivo* experimentations before moving pre-clinical and clinical settings.

4. Conclusion

Green synthesis method using cow dung was successfully established to synthesize CD-TiO_2 and P-CD-TiO_2 nanoparticles which were spherical shaped with the average size ranging from $32-48$ nm respectively. Both of these nanoparticles demonstrated good anti-oxidant, anti-inflammatory, and anti-hemolytic properties. In a dose-dependent manner, considerable cytotoxic activity against Hep3B cells was detected, with P-CD-TiO_2 nanoparticles demonstrating significantly greater activity than CD-TiO_2 nanoparticles. There are several potential uses for this innovative green synthesis method based on cow dung in the realm of nanoparticle-mediated cancer research. Finally, we draw the conclusion that our green produced TiO_2 nanoparticles are less toxic, easier to get, affordable, and environmentally friendly than those derived from other industrial sources. This makes them suitable for use in effective therapeutic applications against HCC, which calls for more study.

Acknowledgments

The author, Sancharan Acharya, gratefully acknowledges the UGC, India for the University fellowship. DST-FIST.

Authors contributions

Authors have contributed equally in preparing and writing the manuscript.

Availability of data and materials

The authors declare that the data supporting the findings of this study are available within the paper.

Conflict of interests

The authors assert that they do not have any identifiable conflicting financial interests or personal relationships that might be perceived to influence the work presented in this paper.

References

[1] K. O. Asafo-Agyei and H. Samant. "Hepatocellular Carcinoma.". *StatPearls. StatPearls Publishing, Treasure Island (FL).*, 2024.

[2] S. Daher, M. Massarwa, A. A. Benson, and T. Khoury. "Current and Future Treatment of Hepatocellular Carcinoma: An Updated Comprehensive Review.". *J Clin Transl Hepatol*, 6:69–78, 2018. DOI: https://doi.org/10.14218/JCTH.2017.00031.

[3] K. Krukiewicz and J. K. Zak. "Biomaterial-based regional chemotherapy: Local anticancer drug delivery to enhance chemotherapy and minimize its side-effects.". *Mater Sci Eng C*, 62:927–942, 2016. DOI: https://doi.org/10.1016/j.msec.2016.01.063.

[4] S. Anandhakumar, G. Krishnamoorthy, K. M. Ramkumar, and A. M. Raichur. "Preparation of collagen peptide functionalized chitosan nanoparticles by ionic gelation method: An effective carrier system for encapsulation and release of doxorubicin for cancer drug delivery.". *Mater Sci Eng C*, 70:378–385, 2017. DOI: https://doi.org/10.1016/j.msec.2016.09.003.

[5] A. Muthuvel, N. M. Said, M. Jothibas, K. Gurushankar, and V. Mohana. "Microwave-assisted green synthesis of nanoscaled titanium oxide: photocatalyst, antibacterial and antioxidant properties.". *J Mater Sci Mater Electron*, 32:23522–23539, 2021. DOI: https://doi.org/10.1007/s10854-021-06840-3.

[6] A. B. Younis, Y. Haddad, L. Kosaristanova, and K. Smerkova. "Titanium dioxide nanoparticles: Recent progress in antimicrobial applications.". *WIREs Nanomedicine Nanobiotechnology*, 15:e1860, 2023. DOI: https://doi.org/10.1002/wnan.1860.

[7] Y. Mbenga, J. O. Adeyemi, D. M. N. Mthiyane, M. Singh, and D. C. Onwudiwe. "Green synthesis, antioxidant and anticancer activities of TiO2 nanoparticles using aqueous extract of *Tulbhagia violacea*.". *Results Chem*, 6:101007, 2023. DOI: https://doi.org/10.1016/j.rechem.2023.101007.

[8] Catalysts — Free Full-Text — Photocatalytic Water Treatment by Titanium Dioxide: Recent Updates. 2024. URL https://www.mdpi.com/2073-4344/2/4/572.

[9] V. Verma, M. Al-Dossari, J. Singh, M. Rawat, M. G. M. Kordy, and M. Shaban. "A Review on Green Synthesis of TiO_2 NPs: Photocatalysis and Antimicrobial Applications.". *Polymers*, 14:1444, 2022. DOI: https://doi.org/10.3390/polym14071444.

[10] A. S. Abdellatef, A. Ohi, T. Nabatame, and A. Taniguchi. "Induction of hepatocyte functional protein expression by submicron/nanopatterning substrates to mimic in vivo structures.". *Biomater Sci*, 2: 330–338, 2014. DOI: https://doi.org/10.1039/C3BM60191A.

[11] T. Sree Latha, M. C. Reddy, S. V. Muthukonda, V. V. S. S. Srikanth, and D. Lomada. "In vitro and in vivo evaluation of anti-cancer activity: Shape-dependent properties of TiO_2 nanostructures.". *Mater Sci Eng C*, 78:969–977, 2017.
DOI: https://doi.org/10.1016/j.msec.2017.04.011.

[12] A.-P. Zhang and Y.-P. Sun. "Photocatalytic killing effect of TiO_2 nanoparticles on Ls-174-t human colon carcinoma cells.". *World J Gastroenterol WJG*, 10:3191–3193, 2004.
DOI: https://doi.org/10.3748/wjg.v10.i21.3191.

[13] K. Takaki, Y. Higuchi, M. Hashii, C. Ogino, and N. Shimizu. "Induction of apoptosis associated with chromosomal DNA fragmentation and caspase-3 activation in leukemia L1210 cells by TiO_2 nanoparticles.". *J Biosci Bioeng*, 117:129–133, 2014.
DOI: https://doi.org/10.1016/j.jbiosc.2013.06.003.

[14] Z. Javed, G. D. Tripathi, M. Mishra, M. Gattupalli, and K. Dashora. "Cow dung extract mediated green synthesis of zinc oxide nanoparticles for agricultural applications.". *Sci Rep*, 12:20371, 2022.
DOI: https://doi.org/10.1038/s41598-022-22099-y.

[15] M. Thatyana, N. P. Dube, D. Kemboi, A. L. E. Manicum, N. S. Mokgalaka-Fleischmann, and J. V. Tembu. "Advances in Phytonanotechnology: A Plant-Mediated Green Synthesis of Metal Nanoparticles Using Phyllanthus Plant Extracts and Their Antimicrobial and Anticancer Applications.". *Nanomaterials*, 13:2616, 2023.
DOI: https://doi.org/10.3390/nano13192616.

[16] Y. Chen, G. Wang, H. Wang, C. Cheng, G. Zang, X. Guo, and R. H. Liu. "Phytochemical Profiles and Antioxidant Activities in Six Species of Ramie Leaves.". *PLOS ONE*, 9:e108140, 2014.
DOI: https://doi.org/10.1371/journal.pone.0108140.

[17] A. Razzaz, S. Ghorban, L. Hosayni, M. Irani, and M. Aliabadi. "Chitosan nanofibers functionalized by TiO_2 nanoparticles for the removal of heavy metal ions.". *J Taiwan Inst Chem Eng*, 58:333–343, 2016.
DOI: https://doi.org/10.1016/j.jtice.2015.06.003.

[18] S. Tharani, D. Bharathi, and R. Ranjithkumar. "Extracellular green synthesis of chitosan-silver nanoparticles using Lactobacillus reuteri for antibacterial applications.". *Biocatal Agric Biotechnol*, 30: 101838, 2020.
DOI: https://doi.org/10.1016/j.bcab.2020.101838.

[19] X. X. Li, C. Liu, S. L. Dong, C. S. Ou, J. L. Lu, J. H. Ye, Y. R. Liang, and X. Q. Zheng. "Anticarcinogenic potentials of tea catechins.". *Front Nutr*, 9:1060783, 2022.
DOI: https://doi.org/10.3389/fnut.2022.1060783.

[20] S. W. Kim, Y. W. Han, S. T. Lee, H. J. Jeong, S. H. Kim, I. H. Kim, S. O. Lee, D. G. Kim, S. H. Kim, S. Z. Kim, and W. H. Park. "A superoxide anion generator, pyrogallol, inhibits the growth of HeLa cells via cell cycle arrest and apoptosis.". *Mol Carcinog*, 47:114–125, 2008.
DOI: https://doi.org/10.1002/mc.20369.

[21] G. Sampath, D. J. H. Shyu, N. Rameshkumar, M. Krishnan, P. Sivasankar, and N. Kayalvizhi. "Synthesis and Characterization of Pyrogallol Capped Silver Nanoparticles and Evaluation of Their In Vitro Anti-Bacterial, Anti-cancer Profile Against AGS Cells.". *J Clust Sci*, 32:549–557, 2021.
DOI: https://doi.org/10.1007/s10876-020-01813-8.

[22] N. Kancherla, A. Dhakshinamoothi, K. Chitra, and R. B. Komaram. "Preliminary Analysis of Phytoconstituents and Evaluation of Anthelminthic Property of Cayratia auriculata (In Vitro).". *Mædica*, 14: 350–356, 2019.
DOI: https://doi.org/10.26574/maedica.2019.14.4.350.

[23] S. Pooja. Gm V Phytochemical screening for secondary metabolites of Opuntia dillenii Haw.

[24] S. Manhas, C. Attri, M. Seth, and A. Seth. "Determination of phytochemical constituents and evaluation of antimicrobial activity of medicinal fern Christella dentata.". *Int J Mol Sci*, 35:169–178, 2018.
DOI: https://doi.org/Indian Fern Journal.

[25] O. Folin and W. Denis. "A Colorimetric method for the determination of phenols (and phenol derivatives) in Urine.". *J Biol Chem*, 22: 305–308, 1915.
DOI: https://doi.org/10.1016/S0021-9258(18)87648-7.

[26] N. Liaqat, N. Jahan, Khalil ur Rahman, T. Anwar, and H. Qureshi. "Green synthesized silver nanoparticles: Optimization, characterization, antimicrobial activity, and cytotoxicity study by hemolysis assay.". *Front Chem.*, 10, 2022.
DOI: https://doi.org/10.3389/fchem.2022.952006.

[27] J. L. Lopez-Miranda, G. A. Molina, M. A. González-Reyna, B. L. España-Sánchez, R. Esparza, R. Silva, and M. Estévez. "Antibacterial and Anti-Inflammatory Properties of ZnO Nanoparticles Synthesized by a Green Method Using Sargassum Extracts.". *Int J Mol Sci*, 24: 1474, 2023.
DOI: https://doi.org/10.3390/ijms24021474.

[28] G. Rajakumar, M. Thiruvengadam, G. Mydhili, T. Gomathi, and I. M. Chung. "Green approach for synthesis of zinc oxide nanoparticles from Andrographis paniculata leaf extract and evaluation of their antioxidant, anti-diabetic, and anti-inflammatory activities.". *Bioprocess Biosyst Eng*, 41:21–30, 2018.
DOI: https://doi.org/10.1007/s00449-017-1840-9.

[29] M. A. Solaiman, M. A. Ali, N. M. Abdel-Moein, and E.A. Mahmoud. "Synthesis of Ag-NPs developed by green-chemically method and evaluation of antioxidant activities and anti-inflammatory of synthesized nanoparticles against LPS-induced NO in RAW 264.7 macrophages.". *Biocatal Agric Biotechnol*, 29:101832, 2020.
DOI: https://doi.org/10.1016/j.bcab.2020.101832.

[30] P. B. Ezhuthupurakkal, S. Ariraman, S. Arumugam, N. Subramaniyan, S. K. Muthuvel, P. Kumpati, B. Rajamani, and T. Chinnasamy. "Anticancer potential of ZnO nanoparticle-ferulic acid conjugate on Huh-7 and HepG2 cells and diethyl nitrosamine induced hepatocellular cancer on Wistar albino rat.". *Nanomedicine Nanotechnol Biol Med*, 14:415–428, 2018.
DOI: https://doi.org/10.1016/j.nano.2017.11.003.

[31]

[32] R. Dobrucka. "Synthesis of Titanium Dioxide Nanoparticles Using Echinacea purpurea Herba.". *Iran J. Pharm. Res.*, 16:756–762, 2017.

[33] N. K. Ahmed, A. Abbady, Y. A. Elhassan, and A. H. Said. "Green Synthesized Titanium Dioxide Nanoparticle from Aloe Vera Extract as a Promising Candidate for Radiosensitization Applications.". *BioNanoScience*, 13:730–743, 2023.
DOI: https://doi.org/10.1007/s12668-023-01085-2.

[34] M. Canillas, E. Chinarro, M. Freitas, A. P. Pêgo, and B. Moreno. "Titanium dioxide catalytic activity contributes to the process of free radical scavenging.". *J Catal*, 381:186–192, 2020.
DOI: https://doi.org/10.1016/j.jcat.2019.09.030.

[35] N. Yuangpho, S. T. T. Le, T. Treerujiraphapong, W. Khanitchaidecha, and A. Nakaruk. "Enhanced photocatalytic performance of TiO_2 particles via effect of anatase–rutile ratio.". *Phys E Low-Dimens Syst Nanostructures*, 67:18–22, 2015.
DOI: https://doi.org/10.1016/j.physe.2014.11.006.

[36] A. Li Bassi, D. Cattaneo, V. Russo, C. E. Bottani, E. Barborini, T. Mazza, P. Piseri, P. Milani, F. O. Ernst, K. Wegner, and Pratsinis S. E. "Raman spectroscopy characterization of titania nanoparticles produced by flame pyrolysis: The influence of size and stoichiometry.". *J Appl Phys*, 98:074305, 2005.
DOI: https://doi.org/10.1063/1.2061894.

[37] H. C. Choi, Y. M. Jung, and S. B. Kim. "Size effects in the Raman spectra of TiO_2 nanoparticles.". *Vib Spectrosc*, 37:33–38, 2005.
DOI: https://doi.org/10.1016/j.vibspec.2004.05.006.

[38] H. Ming, H. Zhang, Z. Ma, H. Huang, S. Lian, Y. Wei, Y. Liu, and Z. Kang. "Scanning transmission X-ray microscopy, X-ray photoelectron spectroscopy, and cyclic voltammetry study on the enhanced visible photocatalytic mechanism of carbon–TiO_2 nanohybrids.". *Appl Surf Sci*, 258:3846–3853, 2012.
DOI: https://doi.org/10.1016/j.apsusc.2011.12.043.

[39] O. Ouerghi, M. H. Geesi, Y. Riadi, and E. O. Ibnouf. "Limon-citrus extract as a capping/reducing agent for the synthesis of titanium dioxide nanoparticles: characterization and antibacterial activity. ". *Green Chem Lett Rev*, 15:483–490, 2022.
DOI: https://doi.org/10.1080/17518253.2022.2094205.

[40] N. Ajmal, K. Saraswat, M. D. A. Bakht, Y. Riadi, M. J. Ahsan, and M. D. Noushad. "Cost-effective and eco-friendly synthesis of titanium dioxide (TiO_2) nanoparticles using fruit's peel agro-waste extracts: characterization, *in vitro* antibacterial, antioxidant activities.". *Green Chem Lett Rev*, 12:244–254, 2019.
DOI: https://doi.org/10.1080/17518253.2019.1629641.

[41] R. Rajendhiran, V. Deivasigamani, J. Palanisamy, S. Pitchaiya, N. Eswaramoorthy, and S. Masan. "Plectranthus amboinicus Leaf Extract Synthesized Spherical like-TiO_2 Photoanode for Dye-Sensitized Solar Cell Application.". *Silicon*, 13:3329–3336, 2021.
DOI: https://doi.org/10.1007/s12633-020-00709-6.

[42] S. S. Mathew, N. E. Sunny, and V. Shanmugam. "Green synthesis of anatase titanium dioxide nanoparticles using Cuminum cyminum seed extract; effect on Mung bean (Vigna radiata) seed germination.". *Inorg Chem Commun*, 126:108485, 2021.
DOI: https://doi.org/10.1016/j.inoche.2021.108485.

[43] A. Chahardoli, H. Sharifan, N. Karimi, and S. N. Kakavand. "Uptake, translocation, phytotoxicity, and hormetic effects of titanium dioxide nanoparticles (TiO_2NPs) in Nigella arvensis L..". *Sci Total Environ*, 806:151222, 2022.
DOI: https://doi.org/10.1016/j.scitotenv.2021.151222.

[44] S. Mahalakshmi and P. Vijaya. "Evaluation of In-vitro Biocompatibility and Antimicrobial activities of Titanium Dioxide (TiO_2) Nanoparticles by Hydrothermal Method.". *Nano Biomed Eng*, 13: 378–385, 2021.
DOI: https://doi.org/10.5101/nbe.v13i1.p36-43.

[45] H. Gul, H. M. A. Javed, M. Awais, M. Y. Javaid, M. I. Khan, M. Arif, M. Y. Alshahrani, R. M. A. Khalil, F. S. Khan, and A. M. Galal. "TiO_2 nanoparticles functionalized with marigold for antioxidant role to enhance the skin protection.". *Biomass Convers Biorefinery*, 13: 16025–16035, 2023.
DOI: https://doi.org/10.1007/s13399-022-02433-0.

[46] D. Dekanski, B. Spremo-Potparević, V. Bajić, L. Živković, D. Topalović, D. N. Sredojević, V. Lazić, and J. M. Nedeljković. "Acute toxicity study in mice of orally administrated TiO_2 nanoparticles functionalized with caffeic acid.". *Food Chem Toxicol*, 115: 42–48, 2023.
DOI: https://doi.org/10.1016/j.fct.2018.02.064.

[47] H. Agarwal, A. Nakara, and V. K. Shanmugam. "Anti-inflammatory mechanism of various metal and metal oxide nanoparticles synthesized using plant extracts: A review.". *Biomed Pharmacother*, 109: 2561–2572, 2019.
DOI: https://doi.org/10.1016/j.biopha.2018.11.116.

[48] M. Alavi and N. Karimi. "Characterization, antibacterial, total antioxidant, scavenging, reducing power and ion chelating activities of green synthesized silver, copper and titanium dioxide nanoparticles using Artemisia haussknechtii leaf extract.". *Artif Cells Nanomedicine Biotechnol*, 46:2066–2081, 2018.
DOI: https://doi.org/10.1080/21691401.2017.1408121.

[49] C. Y. Jin, B. S. Zhu, X. F. Wang, and Q. H. Lu. "Cytotoxicity of Titanium Dioxide Nanoparticles in Mouse Fibroblast Cells.". *Chem Res Toxicol*, 21:1871–1877, 2008.
DOI: https://doi.org/10.1021/tx800179f.

[50] X. Wei, Y. Liu, A. El-kott, A. E. Ahmed, and A. Khames. "Calendula officinalis-based green synthesis of titanium nanoparticle: Fabrication, characterization, and evaluation of human colorectal carcinoma.". *J Saudi Chem Soc*, 25:101343, 2021.
DOI: https://doi.org/10.1016/j.jscs.2021.101343.

[51] Y Wang, H. Cui, J. Zhou, F. Li, J. Wang, M. Chen, and Q. Liu. "Cytotoxicity, DNA damage, and apoptosis induced by titanium dioxide nanoparticles in human non-small cell lung cancer A549 cells.". *Environ Sci Pollut Res*, 22:5519–5530, 2015.
DOI: https://doi.org/10.1007/s11356-014-3717-7.

[52] Z. Mohammadalipour, M. Rahmati, A. Khataee, and M. A. Moosavi. "Different Concentrations of Titanium Dioxide Nanoparticles Induce Autophagy Followed by Growth Inhibition or Cell Death in A375 Melanoma Cells.". *J Skin Stem Cell*, 4, 2017.
DOI: https://doi.org/10.5812/jssc.63994.

[53] J. Zhao, L. Bowman, X. Zhang, V. Vallyathan, S. H. Young, V. Castranova, and M. Ding. "itanium Dioxide (TiO_2) Nanoparticles Induce JB6 Cell Apoptosis Through Activation of the Caspase-8/Bid and Mitochondrial Pathways.". *J Toxicol Environ Health A*, 72:1141–1149, 2009.
DOI: https://doi.org/10.1080/15287390903091764.

[54] S. Ranjan, N. Dasgupta, D. Mishra, and C. Ramalingam. "Involvement of Bcl-2 Activation and G1 Cell Cycle Arrest in Colon Cancer Cells Induced by Titanium Dioxide Nanoparticles Synthesized by Microwave-Assisted Hybrid Approach.". *Front Bioeng Biotechnol*, 8, 2020.
DOI: https://doi.org/10.3389/fbioe.2020.00606.

[55] B. Crivelli, E. Bari, S. Perteghella, L. Catenacci, M. Sorrenti, M. Mocchi, S. Faragò, G. Tripodo, A. Prina-Mello, and M. L. Torre. "Silk fibroin nanoparticles for celecoxib and curcumin delivery: ROS-scavenging and anti-inflammatory activities in an *in vitro* model of osteoarthritis.". *Eur J Pharm Biopharm*, 137:37–45, 2019.
DOI: https://doi.org/10.1016/j.ejpb.2019.02.008.